Inverse Problems and Imaging
Volume 11, No. 5, 2017, 901–916
doi:10.3934/ipi.2017042

A DIRECT IMAGING METHOD FOR THE HALF-SPACE INVERSE SCATTERING PROBLEM WITH PHASELESS DATA

Zhiming Chen

LSEC, Institute of Computational Mathematics and Scientific/Engineering Computing
Academy of Mathematics and Systems Science
School of Mathematical Science, University of Chinese Academy of Sciences
Chinese Academy of Sciences, Beijing 100190, China

Shaofeng Fang

School of Mathematical Science
University of Chinese Academy of Sciences
Chinese Academy of Sciences, Beijing 100190, China

Guanghui Huang*

The Rice Inversion Project
Department of Computational and Applied Mathematics
Rice University, Houston, TX 77005-1892, USA

(Communicated by Jun Zou)

Abstract. We propose a direct imaging method based on the reverse time migration method for finding extended obstacles with phaseless total field data in the half space. We prove that the imaging resolution of the method is essentially the same as the imaging results using the scattering data with full phase information when the obstacle is far away from the surface of the half-space where the measurement is taken. Numerical experiments are included to illustrate the powerful imaging quality.

1. **Introduction.** In this paper, we study a direct imaging method for finding the support of an unknown extended obstacle embedded in the half space using the amplitude of the total field, which is measured on the boundary of half space far away from the obstacle. The algorithm does not require any a priori information of the physical properties of the obstacle such as penetrable or non-penetrable, and for non-penetrable obstacles, the type of boundary conditions on the boundary of the obstacle.

Let the penetrable obstacle occupy a bounded Lipschitz domain $D \subset \mathbb{R}^2_+ = \{(x_1, x_2)^T : x_1 \in \mathbb{R}, x_2 > 0\}$ with ν the unit outer normal to its boundary Γ_D. We assume the incident wave is emitted by a point source located at x_s on the surface $\Gamma_0 = \{(x_1; x_2)^T : x_1 \in \mathbb{R}, x_2 = 0\}$. Let $N(x, y)$ be the Neumann Green function of the Hemholtz equation in the half space,

$$N(x, y) = \Phi(x, y) + \Phi(x, y'), \tag{1}$$

2010 *Mathematics Subject Classification.* Primary: 65N30; Secondary: 78A45, 35Q60.
Key words and phrases. Reverse time migration, phaseless imaging, half-space inverse scattering.
The first author was supported in part by the China NSF under the grant 113211061.
* Corresponding author: Guanghui Huang.

where $\Phi(x,y)=\frac{\mathbf{i}}{4}H_0^{(1)}(k|x-y|)$ is the fundamental solution of the Hemholtz equation, and $y'=(y_1,-y_2)^T$ is the image point of $y=(y_1,y_2)^T\in\mathbb{R}^2_+$. The total field is $u(x,x_s)=N(x,x_s)+u^s(x,x_s)$, where $u^s(x,x_s)$ is the solution of

$$\Delta u^s(x,x_s)+k^2n(x)u^s(x,x_s)=-k^2(n(x)-1)N(x,x_s)\quad\text{in}\quad\mathbb{R}^2_+, \tag{2}$$

$$\frac{\partial u^s}{\partial x_2}(x,x_s)=0\quad\text{on}\quad\Gamma_0, \tag{3}$$

$$\sqrt{r}\left(\frac{\partial u^s}{\partial r}-\mathbf{i}ku^s\right)\to 0\quad\text{as}\quad r\to\infty,\quad r=|x|, \tag{4}$$

where $k>0$ is the wave number, $n(x)\in L^\infty(\mathbb{R}^2_+)$ is a positive scalar function which is equal to 1 outside the scatter D. Condition (4) is the well known Sommerfeld radiation condition which guarantees the uniqueness of the solution. In this paper, by the scattering problem or scattering solution we always mean the solution satisfies the Sommerfeld radiation condition (4) .

In the diffractive optics imaging and radar imaging systems, measurement of the intensity of the total field is much easier and cheaper than the phase information of the field [13, 14]. There are two types of approaches proposed in the literature to solve the inverse scattering problems with phaseless data. The first kind of approach is first to apply the phase retrieval algorithm to extract the phase information of the scattering field from the measurement of the intensity and then use the retrieved full field data in the classical imaging algorithms, see e.g. [15, 2, 24]. The second one is the iterative method which directly minimizes the difference between the received amplitude of the far field pattern and the synthesized phaseless data in the least square sense [19, 17, 18, 1, 5].

The reverse time migration (RTM) method, which consists of back-propagating the complex conjugated scattering field into the background medium and computing the crosscorrelation between the incident wave field and the backpropagated field to output the final imaging profile, is nowadays a standard imaging technique widely used in seismic imaging [3]. In [7, 8, 9], the RTM method for reconstructing extended targets using acoustic, electromagnetic and elastic waves at a fixed frequency is proposed and studied. Without using the small inclusion or geometrical optics assumption previously made in the literature, it is shown in [7, 8, 9] that the RTM imaging function is the total far field pattern of the scattering solution with the imaginary part of the fundamental solution as the incoming wave. This implies the RTM imaging function will always peak on the boundary of the scatterer.

We also remark that several direct sampling schemes for locating multiple multiscale acoustic scatterers are proposed in a very general and practical setting in [20, 23], which are fast and robust against measurement noise. We also refer to [21, 22] for direct sampling approaches to recover multiscale electromagnetic scatterers located in a homogeneous space.

In [11], the first attempt to apply direct imaging method using the idea of RTM method with phaseless data is made. It is shown that the proposed phaseless imaging function can achieve the same resolution as the RTM method applied to full phase data in [7]. The idea of developing direct imaging methods based on RTM has been extended to the electromagnetic waves in [12].

In this paper we study the phaseless imaging method in the half space since in practical applications, one may only be able to access the amplitude of the scattering data in the limited aperture. In [10], the RTM method for finding the extended

obstacle embedded in the half space from scattering data with full phase information has been proposed and the resolution analysis is also proved under proper conditions. The half-space imaging function in [10] can be viewed as the frequency domain counterpart of the time domain imaging function previously proposed in the literature [27, 26].

We denote by Ω the sampling domain in which the obstacle is sought. Let $h = \text{dist}(\Omega, \Gamma_0)$ be the distance of Ω to Γ_0. Let $u^i(x, x_s) = N(x, x_s)$, with the source x_s at $\Gamma_0^d = \{(x_1, x_2)^T; x_1 \in (-d, d), x_2 = 0\}$, where $d > 0$ is the aperture. Let $u^s(x, x_s)$ be the scattering solution of (2) − (3). The RTM imaging function proposed in [10] using full phase scattering data for imaging extended targets in the half space is given by,

$$I_{\text{RTM}}(z) = \text{Im} \int_{\Gamma_0^d} \int_{\Gamma_0^d} \frac{\partial \Phi(x_s, z)}{\partial x_2(x_s)} \frac{\partial \Phi(x_r, z)}{\partial x_2(x_r)} \overline{u^s(x_r, x_s)} ds(x_r) ds(x_s), \quad \forall z \in \Omega. \tag{5}$$

It is shown in [10] that this imaging function always peaks on the upper boundary of the obstacle.

In this paper, inspired by [11] we propose the following imaging function based on RTM for imaging obstacles with only intensity measurement $|u(x_r, x_s)|$:

$$I_{\text{RTM}}^{\text{Phaseless}}(z) = \text{Im} \int_{\Gamma_0^d} \int_{\Gamma_0^d} \frac{\partial \Phi(x_s, z)}{\partial x_2(x_s)} \frac{\partial \Phi(x_r, z)}{\partial x_2(x_r)} \Delta(x_r, x_s) ds(x_r) ds(x_s), \quad \forall z \in \Omega. \tag{6}$$

where

$$\Delta(x_r, x_s) = \frac{|u(x_r, x_s)|^2 - |u^i(x_r, x_s)|^2}{u^i(x_r, x_s)}. \tag{7}$$

We will show in Theorem 4.1 below that

$$I_{\text{RTM}}^{\text{Phaseless}}(z) = I_{\text{RTM}}(z) + O\left(\frac{1}{\sqrt{kh}}\right), \quad \forall z \in \Omega. \tag{8}$$

Therefore the imaging resolution of our new phaseless RTM algorithm is essentially the same as the imaging results using the scattering data with the full phase information when the sources and measurements are placed far away from the scatterer.

The rest of this paper is organized as follows. In section 2 we introduce our half-space RTM algorithm for imaging the obstacle with phaseless data. In section 3 we introduce some preliminary results. In section 4 we consider the resolution of our algorithm for imaging penetrable obstacles. In section 5 we extend our theoretical results to non-penetrable obstacles with sound soft, sound hard, and impedance boundary condition. In section 6 we report several numerical examples to show the competitive performance of our phaseless RTM algorithm.

2. Reverse time migration algorithm.

In this section, we introduce the phaseless RTM method for inverse acoustic scattering problems in the half space. Assume that there are N_s sources and N_r receivers uniformly distributed on Γ_0^d, where $\Gamma_0^d = \{(x_1, x_2)^T : x_1 \in (-d, d), x_2 = 0\}$, where $d > 0$ is the aperture. We always assume the obstacle $D \subset \Omega$.

Let $u^i(x, x_s) = N(x, x_s)$ be the incident wave with source at $x_s \in \Gamma_0^d$, and $|u(x_r, x_s)| = |u^s(x_r, x_s) + u^i(x_r, x_s)|$ be the phaseless total data received at $x_r \in \Gamma_0^d$, where $u^s(\cdot, x_s)$ is the scattering solution of (2)-(3). We always assume that $x_s \neq x_r$ for all $s = 1,\ldots,N_s$, $r = 1,\ldots,N_r$, to avoid the singularity of the incident field $u^i(x, x_s)$ at $x = x_r$. This assumption can be easily satisfied in practical applications.

The phaseless RTM algorithm consists of back-propagating the corrected data $\Delta(x_r, x_s)$ into the sampling domain using $\frac{\partial\Phi(x_r,z)}{\partial x_2(x_r)}$, and then computing the imaginary part of the cross-correlation between $\frac{\partial\Phi(x_s,z)}{\partial x_2(x_s)}$ and the back-propagated field.

Algorithm 2.1. (PHASELESS RTM IN THE HALF SPACE) Given the data $|u(x_r, x_s)|=|u^s(x_r, x_s) + u^i(x_r, x_s)|$ which is the measured amplitude of the total field at $x_r \in \Gamma_0^d$, when the point source is emitted at $x_s \in \Gamma_0^d$.
1° Back-propagation: For $s = 1, \ldots, N_s$, compute the back-propagation field

$$v_b(z, x_s) = \frac{|\Gamma_0^d|}{N_r} \sum_{r=1}^{N_r} \frac{\partial\Phi(x_r, z)}{\partial x_2(x_r)} \Delta(x_r, x_s), \quad \forall z \in \Omega. \tag{9}$$

2° Cross-correlation: For $z \in \Omega$, compute

$$I_d(z) = \mathrm{Im} \left\{ \frac{|\Gamma_0^d|}{N_s} \sum_{s=1}^{N_s} \frac{\partial\Phi(x_s, z)}{\partial x_2(x_s)} v_b(z, x_s) \right\}. \tag{10}$$

It is easy to see that

$$I_d(z) = \mathrm{Im} \left\{ \frac{|\Gamma_0^d||\Gamma_0^d|}{N_s N_r} \sum_{s=1}^{N_s} \sum_{r=1}^{N_r} \frac{\partial\Phi(x_s, z)}{\partial x_2(x_s)} \frac{\partial\Phi(x_r, z)}{\partial x_2(x_r)} \Delta(x_r, x_s) \right\}, \quad \forall z \in \Omega. \tag{11}$$

This formula is used in all the numerical experiments in section 6. By letting $N_s, N_r \to \infty$, we know that it can be viewed as an approximation of the following integral:

$$I_{\mathrm{RTM}}^{\mathrm{Phaseless}}(z) = \mathrm{Im} \int_{\Gamma_0^d} \int_{\Gamma_0^d} \frac{\partial\Phi(x_s, z)}{\partial x_2(x_s)} \frac{\partial\Phi(x_r, z)}{\partial x_2(x_r)} \Delta(x_r, x_s) ds(x_r) ds(x_s), \ \forall z \in \Omega.$$

We will show in section 4 that the above integral is indeed absolutely convergent.

3. **Preliminary results.** We first introduce some notations. For any bounded domain $U \subset \mathbb{R}^2$, let

$$\|u\|_{H^1(U)} = (\|\nabla\phi\|_{L^2(U)}^2 + d_U^{-2}\|\phi\|_{L^2(U)}^2)^{1/2}$$

be the weighted $H^1(U)$ norm, where d_U is the diameter U. We introduce the following stability estimate of the forward acoustic scattering problem for penetrable obstacle in the half space, which can be proved by the same argument as in [4, Theorem 5.26].

Lemma 3.1. *Let $1 - n(x) \in L^\infty(D)$, $g \in L^2(D)$ be scalar functions supported in D, then the scattering problem of Hemholtz equation in the half space*

$$\begin{aligned} \Delta w + k^2 n(x) w &= k^2(1 - n(x))g \quad \text{in} \quad \mathbb{R}^2_+, \\ \frac{\partial w}{\partial x_2} &= 0 \quad \text{on} \quad \Gamma_0, \end{aligned} \tag{12}$$

has a unique radiating solution $w \in H^1(D)$. Moreover, there exists a constant $C > 0$, such that

$$\|w\|_{H^1(D)} \le C\|n\|_{L^\infty(D)}\|g\|_{L^2(D)}. \tag{13}$$

By Lemma 3.1, we can introduce the solution operator $\mathbb{S} : L^2(D) \to H^1(D)$ by $w = \mathbb{S}g$ which maps the incident wave $g \in L^2(D)$ to the scattering field $w \in H^1(D)$. In this paper we will denote by $\|\mathbb{S}\|$ the operator norm of $\mathbb{S}$ which depends generally on $k, n(x)$ and the domain D.

For any $y, z \in \Omega$, define

$$F(z,y) = -\frac{\mathbf{i}}{2\pi}\int_0^\pi e^{\mathbf{i}k(z_1-y_1)\cos\theta+\mathbf{i}k(z_2-y_2)\sin\theta}d\theta.$$

Obviously, $F(z,y) = -\mathbf{i}/2$ if $z = y$. It is shown in [10, Lemma 3.3] that, for some constant C independent of k,

$$|F(z,y)| \le C[(k|z-y|)^{-1/2} + (k|z-y|)^{-1}], \quad \forall z, y \in \Omega. \tag{14}$$

Therefore, $F(z,y)$ shares the same property as the point spread function: peaks when $z = y$ and decays as the $|z-y|$ becomes large. The following theorem for the imaging function $I_{\rm RTM}(z)$ in (5) is given in [10, Theorem 5.2].

Theorem 3.2. *For any $z \in \Omega$, let $\psi(y,z)$ be the radiation solution of the problem*

$$\Delta_y\psi(y,z) + k^2 n(y)\psi(y,z) = -k^2(n(y)-1)\overline{F(z,y)} \quad in \quad \mathbb{R}^2.$$

Then we have, for any $z \in \Omega$,

$$I_{\rm RTM}(z) = -\frac{1}{4}{\rm Im}\int_D k^2(1-n(y))(\psi(y,z)+\overline{F(z,y)})\overline{F(z,y)}dy + W_{\hat{I}}(z),$$

where $\left|W_{\hat{I}}(z)\right| \le C(1+kd_D)^4((kh)^{-1/2}+h/d)$, uniformly for $z \in \Omega$.

We remark that for the penetrable scatterers, $\psi(y,z)$ is the scattering solution with the incoming field $\overline{F(z,y)}$. By (14) we expect the imaging function $I_{\rm RTM}(z)$ will peak on the boundary of the scatterer and decay away from the scatterer. For the sound soft obstacles, when $kh \gg 1$ and $d \gg h$, it is shown in [10] by using the stationary phase theorem and Kirchhoff approximation that one cannot imaging the back part of the obstacle with the scattering data collected only on Γ_0. The extensive numerical examples in [10] confirm the effectiveness of the RTM imaging function $I_{\rm RTM}(z)$ in (5).

4. **Resolution analysis for the phaseless RTM algorithm.** In this section, we prove the following theorem which shows that our RTM algorithm for the half-space phaseless scattering data is asymptotically the same as the RTM algorithm using the scattering data with full phase information. In this section we make the following assumption:

$$|y_1 - z_1| \le Ch, \ z_2 \le Ch, \quad \forall y, z \in \Omega, \quad \text{where } h = \text{dist}(\Omega, \Gamma_0). \tag{15}$$

Theorem 4.1. *If the measured field $|u(x_r,x_s)| = |u^s(x_r,x_s)+u^i(x_r,x_s))|$ with $u^s(x,x_s)$ the scattering solution of (2)-(3) with the incident field $u^i(x,x_s) = N(x, x_s)$, we have*

$$I_{\rm RTM}^{\rm phaseless}(z) = I_{\rm RTM}(z) + R_{\rm RTM}^{\rm phaseless}(z), \quad \forall z \in \Omega,$$

where

$$\left|R_{\rm RTM}^{\rm phaseless}(z)\right| \le C(1+\|\mathbb{S}\|)^2(kh)^{-1/2}, \quad \forall z \in \Omega.$$

Here the constant C may dependent on kd_D and $\|n(\cdot)\|_{L^\infty(D)}$, but is independent of k, h, d_D.

We remark that $\|\mathbb{S}\|$ includes complicated dependence on k and the domain D in the stability estimate of the forward scattering problem. The constant C in the theorem may depend on the dimensionless constant kd_D, but it does not depend on k or d_D separately.

The proof of Theorem 4.1 depends on several lemmas that follow. We first observe that

$$\Delta(x_r,x_s)=\overline{u^s(x_r,x_s)}+\frac{|u^s(x_r,x_s)|^2}{u^i(x_r,x_s)}+\frac{u^s(x_r,x_s)\overline{u^i(x_r,x_s)}}{u^i(x_r,x_s)}.$$

This yields

$$\begin{aligned}
&I_{\mathrm{RTM}}^{\mathrm{Phaseless}}(z)\\
=&\mathrm{Im}\int_{\Gamma_0^d}\int_{\Gamma_0^d}\frac{\partial\Phi(x_s,z)}{\partial x_2(x_s)}\frac{\partial\Phi(x_r,z)}{\partial x_2(x_r)}\overline{u^s(x_r,x_s)}ds(x_r)ds(x_s)\\
&+\mathrm{Im}\int_{\Gamma_0^d}\int_{\Gamma_0^d}\frac{\partial\Phi(x_s,z)}{\partial x_2(x_s)}\frac{\partial\Phi(x_r,z)}{\partial x_2(x_r)}\frac{|u^s(x_r,x_s)|^2}{u^i(x_r,x_s)}ds(x_r)ds(x_s)\\
&+\mathrm{Im}\int_{\Gamma_0^d}\int_{\Gamma_0^d}\frac{\partial\Phi(x_s,z)}{\partial x_2(x_s)}\frac{\partial\Phi(x_r,z)}{\partial x_2(x_r)}\frac{u^s(x_r,x_s)\overline{u^i(x_r,x_s)}}{u^i(x_r,x_s)}ds(x_r)ds(x_s)\\
:=&I_{\mathrm{RTM}}(z)+\mathrm{I}_2+\mathrm{I}_3
\end{aligned}\tag{16}$$

Our goal now is to show that $\mathrm{I}_2,\mathrm{I}_3$ are small when $kh\gg 1$. The following estimates for the Hankel functions are proved in [6, (1.22)-(1.23)].

Lemma 4.2. *We have*

$$|H_0^{(1)}(t)|\le\left(\frac{1}{\pi t}\right)^{\frac{1}{2}},\quad |H_1^{(1)}(t)|\le\left(\frac{1}{\pi t}\right)^{\frac{1}{2}}+\frac{1}{\pi t},\quad \forall t>0.$$

Lemma 4.3. *For any $x_s,x_r\in\Gamma_0^d$, we have*

$$|u^s(x_r,x_s)|\le C(1+\|\mathbb{S}\|)[kd(x_r,D)]^{-1/2}[kd(x_s,D)]^{-1/2},$$

where $d(x,D)=\min_{y\in\bar{D}}|x-y|$ is the distance between $x\in\Gamma_0^d$ and D, and the constant C may depend on $kd_D,\|n(\cdot)\|_{L^\infty(D)}$, but is independent of k,d_D.

Proof. By the integral representation theorem

$$u^s(x_r,x_s)=k^2\int_D[n(y)-1]N(x_r,y)[u^s(y,x_s)+N(y,x_s)]ds(y).$$

This implies by Lemma 3.1 that

$$|u^s(x_r,x_s)|\le Ck^2\|n\|_{L^\infty(D)}(1+\|\mathbb{S}\|)\|N(x_r,\cdot)\|_{L^2(D)}\|N(\cdot,x_s)\|_{L^2(D)}.$$

By Lemma 4.2 we have for any $x_r\in\Gamma_0^d,y\in D$, $|N(x_r,y)|=2|\Phi(x_r,y)|\le(k|x_r-y|)^{-1/2}\le[kd(x_r,D)]^{-1/2}$. Similarly, $|N(y,x_s)|\le[kd(x_s,D)]^{-1/2}$ for any $x_s\in\Gamma_0^d,y\in D$. Thus

$$|u^s(x_r,x_s)|\le C(kd_D)^2\|n\|_{L^\infty(D)}(1+\|\mathbb{S}\|)[kd(x_r,D)]^{-1/2}[kd(x_s,D)]^{-1/2}.$$

This completes the proof. □

Lemma 4.4. *Let $kh\ge 1$ and denote $\Gamma_0^{(a,b)}=\{x\in\Gamma_0:x_1\in(a,b)\}$, where $a,b\in\mathbb{R},a<b$. For any $z\in\Omega$, we have*

$$\left|\int_{\Gamma_0^{(a,b)}}\frac{\partial\Phi(x,z)}{\partial x_2}f(x)ds(x)\right|\le(kz_2)^{1/2}\|f\|_{L^\infty(\Gamma_0^{(a,b)})}.$$

Proof. Since $k|x-z| \geq kh \geq 1$ for any $x \in \Gamma_0^{(a,b)}, z \in \Omega$, by Lemma 4.2 we have

$$\left|\frac{\partial \Phi(x,z)}{\partial x_2}\right| = \left|\frac{\mathbf{i}k}{4} H_1^{(1)}(k|x-z|)\frac{z_2}{|x-z|}\right| \leq \frac{1}{2\sqrt{\pi}}\frac{k^{1/2} z_2}{|x-z|^{3/2}}. \tag{17}$$

Thus by using the transform $t = (x_1 - z_1)/z_2$,

$$\left|\int_{\Gamma_0^{(a,b)}} \frac{\partial \Phi(x,z)}{\partial x_2} f(x) ds(x)\right| \leq \frac{(kz_2)^{1/2}}{2\sqrt{\pi}} \|f\|_{L^\infty(\Gamma_0^{(a,b)})} \int_{-\infty}^{\infty} \frac{1}{(1+t^2)^{3/2}} dt.$$

On the other hand,

$$\int_{-\infty}^{\infty} \frac{1}{(1+t^2)^{3/2}} dt \leq 2\left[1 + \int_1^{\infty} \frac{t}{(1+t^2)^{3/2}} dt\right] = 2(1+1/\sqrt{2}) \leq 2\sqrt{\pi}.$$

This completes the proof. □

Now we can give an estimate of the second term in the right hand side (16).

Lemma 4.5. *Let $kh \geq 1$. For any $z \in \Omega$, we have $|\mathrm{I}_2| \leq C(1+\|\mathbb{S}\|)^2 (kh)^{-1/2}$, for some constant C that may depend on $kd_D, \|n(\cdot)\|_{L^\infty(D)}$, but is independent of k, h, d_D.*

Proof. Denote $\Omega_k = \{(x_r, x_s) \in \Gamma_0^d \times \Gamma_0^d : |x_r - x_s| \leq 1/(2k)\}$. By the estimate in [11, Lemma 3.3], we know

$$|H_0^{(1)}(k|x_r - x_s|)| \geq \frac{2}{5\pi e} |\ln(k|x_r - x_s|)| \geq \frac{2\ln 2}{5\pi e}, \quad \forall (x_r, x_s) \in \Omega_k.$$

Since $d(x, D) \geq h$ for $x \in \Gamma_0^d$, we obtain by Lemma 4.3 that

$$\left|\frac{u^s(x_r, x_s)^2}{u^i(x_r, x_s)}\right| \leq C(1+\|\mathbb{S}\|)^2 (kh)^{-2},$$

which implies by Lemma 4.4 that

$$\left|\iint_{\Omega_k} \frac{\partial \Phi(x_s, z)}{\partial x_2(x_s)} \frac{\partial \Phi(x_r, z)}{\partial x_2(x_r)} \frac{|u^s(x_r, x_s)|^2}{u^i(x_r, x_s)} ds(x_r) d(x_s)\right| \leq C(1+\|\mathbb{S})^2 (kh)^{-1}, \tag{18}$$

where we have used the fact that $z_2 \leq Ch$ for $z \in \Omega$ by the assumption (15).

Next we estimate the integral in $\Gamma_0^d \times \Gamma_0^d \backslash \bar{\Omega}_k$. Since $t|H_0^{(1)}(t)|^2$ is an increasing function of $t > 0$ [25, p. 446], we have for $(x_r, x_s) \in \Gamma_0^d \times \Gamma_0^d \backslash \bar{\Omega}_k$, $|x_r - x_s| \geq 1/(2k)$, and thus

$$|x_r - x_s||u^i(x_r, x_s)|^2 \geq \frac{1}{32} k^{-1} \left|H_0^{(1)}\left(\frac{1}{2}\right)\right|^2 = Ck^{-1}.$$

Since $|x_r - x_s| \leq d(x_r, D) + d(x_s, D)$ and $d(x, D) \geq h$ for $x \in \Gamma_0^d$, we obtain by using Lemma 4.3 again that

$$\left|\frac{u^s(x_r, x_s)^2}{u^i(x_r, x_s)}\right| \leq C(1+\|\mathbb{S}\|)^2 \frac{k^{1/2}|x_r - x_s|^{1/2}}{k^2 d(x_r, D) d(x_s, D)} \leq C(1+\|\mathbb{S})^2 (kh)^{-3/2}.$$

Thus by Lemma 4.4 we have

$$\begin{aligned} &\left|\iint_{\Gamma_0^d \times \Gamma_0^d \backslash \bar{\Omega}_k} \frac{\partial \Phi(x_s, z)}{\partial x_2(x_s)} \frac{\partial \Phi(x_r, z)}{\partial x_2(x_r)} \frac{|u^s(x_r, x_s)|^2}{u^i(x_r, x_s)} ds(x_r) d(x_s)\right| \\ \leq & C(1+\|\mathbb{S}\|)^2 (kh)^{-1/2}. \end{aligned} \tag{19}$$

This completes the proof by combining the estimates (18)-(19). □

We now start at estimating the third term of the right hand side (16). Denote by $\delta = (h/k)^{\frac{1}{2}}$, and we introduce the set $Q_\delta = \{(x_r, x_s) \in \Gamma_0^d \times \Gamma_0^d : \ |x_s - x_r| \le \delta\}$. We will also use the notation that for $x_s, x_r \in R_+^2$,

$$x_s = (x_{1s}, x_{2s}), \quad x_r = (x_{1r}, x_{2r}).$$

Lemma 4.6. *We have, for $z \in \Omega$,*

$$\left| \iint_{Q_\delta} \frac{\partial \Phi(x_s, z)}{\partial x_2(x_s)} \frac{\partial \Phi(x_r, z)}{\partial x_2(x_r)} \frac{u^s(x_r, x_s)\overline{u^i(x_r, x_s)}}{u^i(x_r, x_s)} ds(x_r) d(x_s) \right| \le C(1 + \|\mathbb{S}\|)(kh)^{-1/2},$$

where C may depend on $kd_D, \|n(\cdot)\|_{L^\infty(D)}$, but is independent of k, h, d_D.

Proof. It is obvious that

$$\begin{aligned}
&\iint_{Q_\delta} \frac{\partial \Phi(x_s, z)}{\partial x_2(x_s)} \frac{\partial \Phi(x_r, z)}{\partial x_2(x_r)} \frac{u^s(x_r, x_s)\overline{u^i(x_r, x_s)}}{u^i(x_r, x_s)} ds(x_r) d(x_s) \\
&= \int_{-d}^{-d+\delta} \frac{\partial \Phi(x_s, z)}{\partial x_2(x_s)} \int_{-d}^{x_{1s}+\delta} \frac{\partial \Phi(x_r, z)}{\partial x_2(x_r)} \frac{u^s(x_r, x_s)\overline{u^i(x_r, x_s)}}{u^i(x_r, x_s)} dx_{1r} dx_{1s} \\
&\quad + \int_{-d+\delta}^{d-\delta} \frac{\partial \Phi(x_s, z)}{\partial x_2(x_s)} \int_{x_{1s}-\delta}^{x_{1s}+\delta} \frac{\partial \Phi(x_r, z)}{\partial x_2(x_r)} \frac{u^s(x_r, x_s)\overline{u^i(x_r, x_s)}}{u^i(x_r, x_s)} dx_{1r} dx_{1s} \\
&\quad + \int_{d-\delta}^{d} \frac{\partial \Phi(x_s, z)}{\partial x_2(x_s)} \int_{x_{1s}-\delta}^{d} \frac{\partial \Phi(x_r, z)}{\partial x_2(x_r)} \frac{u^s(x_r, x_s)\overline{u^i(x_r, x_s)}}{u^i(x_r, x_s)} dx_{1r} dx_{1s} \\
&:= \mathrm{II}_1 + \mathrm{II}_2 + \mathrm{II}_3.
\end{aligned} \tag{20}$$

Since $|x_s - z| \ge z_2$ for $x_s \in \Gamma_0^d$, by (17), Lemma 4.3 and Lemma 4.4, we obtain

$$|\mathrm{II}_1| \le \delta \cdot \frac{k^{1/2} z_2}{z_2^{3/2}} \cdot (kz_2)^{1/2} \cdot C(1 + \|\mathbb{S}\|)(kh)^{-1} \le C(1 + \|\mathbb{S}\|)(kh)^{-1/2}.$$

where we have used $\delta = (h/k)^{1/2}$. The other terms can be estimated similarly. This completes the proof. □

To proceed the estimate of the integral in $\Gamma_0^d \times \Gamma_0^d \backslash \bar{Q}_\delta$, we first recall the following von der Corput lemma for the oscillatory integral [16, P.152], [10, Lemma 3.2].

Lemma 4.7. *Let $-\infty < a < b < \infty$, $\lambda > 0$, and u is a C^2 function in (a, b). If $|u'(t)| \ge 1$ for $t \in (a, b)$ and u' is monotone in (a, b), then for any ϕ defined in (a, b) with integrable derivatives*

$$\left| \int_a^b \phi(t) e^{\mathbf{i}\lambda u(t)} dt \right| \le 3\lambda^{-1} \left[|\phi(b)| + \int_a^b |\phi'(t)| dt \right].$$

Lemma 4.8. *For any $a, b \in \mathbb{R}, a < b$, we have*

$$\left| \int_{\Gamma_0^{(a,b)}} \frac{\partial \Phi(x, z)}{\partial x_2} \Phi(x, y) e^{-2\mathbf{i}kx_1} ds(x) \right| \le C(kh)^{-1}, \quad \forall y, z \in \Omega,$$

where C may depend on $kd_D, \|n(\cdot)\|_{L^\infty(D)}$, but is independent of k, h, d_D, a, b.

Proof. By Lemma 4.2 and the asymptotic formula of Hankel functions [25, P.197], for $n = 1, 2$,

$$H_n^{(1)}(t) = \left(\frac{2}{\pi t}\right)^{\frac{1}{2}} e^{\mathbf{i}(t - \frac{n\pi}{2} - \frac{\pi}{4})} + R_n(t), \quad |R_n(t)| \le Ct^{-\frac{3}{2}}, \quad \forall t > 0, \tag{21}$$

we can obtain

$$\frac{\partial\Phi(x,z)}{\partial x_2}\Phi(x,y) = -\frac{1}{8\pi}\frac{z_2}{|x-z|^2}e^{\mathbf{i}k(|x-z|+|x-y|)} + R(x,y,z),$$

where

$$\begin{aligned}|R(x,y,z)| \leq & Ck^{-1}|x-z|^{-1/2}|x-y|^{-3/2} + Ck^{-1}|x-z|^{-3/2}|x-y|^{-1/2} \\ & + \ Ck^{-2}|x-z|^{-3/2}|x-y|^{-3/2}.\end{aligned} \tag{22}$$

It is easy to show that

$$\left|\int_{\Gamma_0^{(a,b)}} R(x,y,z)e^{-2\mathbf{i}kx_1}ds(x)\right| \leq C(kh)^{-1}. \tag{23}$$

We are then left to estimate the following integral

$$\mathrm{III} = \int_{\Gamma_0^{(a,b)}} \frac{z_2}{|x-z|^2}e^{\mathbf{i}k(|x-z|+|x-y|-2x_1)}ds(x).$$

By taking the transform $t = (x_1 - z_1)/z_2$ we obtain

$$\mathrm{III} = e^{-2\mathbf{i}kz_1}\int_{a'}^{b'} \frac{1}{1+t^2}\, e^{\mathbf{i}kz_2v(t)}dt,$$

where $b' = (b-z_1)/z_2, a' = (a-z_1)/z_2$, and

$$v(t) = \sqrt{1+t^2} + \sqrt{(t+t_1)^2+t_2^2} - 2t, \quad t_1 = \frac{x_1-z_1}{z_2}, t_2 = \frac{x_2}{z_2}.$$

By simple calculation we have

$$v'(t) = \frac{t}{\sqrt{1+t^2}} + \frac{t+t_1}{\sqrt{(t+t_1)^2+t_2^2}} - 2, \quad v''(t) = \frac{1}{(1+t^2)^{3/2}} + \frac{t_2^2}{[(t+t_1)^2+t_2^2]^{3/2}}.$$

Let $t_0 = \max(0, -t_1)$. It is easy to see that $v'(t) \leq -1$ for $t \leq t_0$. Thus by Lemma 4.7

$$\left|\int_{a'}^{\min(t_0,b')} \frac{1}{1+t^2}\, e^{\mathbf{i}kz_2v(t)}\right| \leq C(kh)^{-1}. \tag{24}$$

If $t_0 \geq b'$, the proof of the lemma finishes by combining (23) and (24). Otherwise, we let $t_0 < b'$ and obtain by integration by parts

$$\int_{t_0}^{b'} \frac{1}{1+t^2}e^{\mathbf{i}kz_2v(t)}dt = \left[\frac{e^{\mathbf{i}kz_2v(t)}}{\mathbf{i}kz_2(1+t^2)v'(t)}\right]_{t_0}^{b'} - \int_{t_0}^{b'} \frac{-2tv'(t)-(1+t^2)v''(t)}{\mathbf{i}kz_2(1+t^2)^2v'(t)^2}dt.$$

Since $v'(t) \leq -1 + t/\sqrt{1+t^2}$, we have $(1+t^2)v'(t) \leq -1/2, \ \forall t \geq 0$. This implies

$$\left|\int_{t_0}^{b'} \frac{1}{1+t^2}e^{\mathbf{i}kz_2v(t)}dt\right| \leq C(kh)^{-1} + C(kh)^{-1}\int_{t_0}^{b'} |2tv'(t)+(1+t^2)v''(t)|dt.$$

Now denote $v = v_1 + v_2$, where

$$v_1(t) = \sqrt{1+t^2} - t, \quad v_2(t) = \sqrt{(t+t_1)^2+t_2^2} - t.$$

Write $\Delta = [(t+t_1)^2+t_2^2]^{1/2}$, by simple calculation,

$$2tv_2'(t) + (1+t^2)v_2''(t) = \frac{t_2^2\,[-2t\Delta^2 + (1+t^2)(t+t_1+\Delta)]}{\Delta^3[t+t_1+\Delta]}.$$

The key observation is that for $t \geq t_0$, $t+t_1 \geq 0$, we have $|2tv_2'(t)+(1+t^2)v_2''(t)| \leq Ct^2/\Delta^4 \leq C\Delta^{-2}$, where we have used $|t_1| \leq C$ by (15). Similarly, $|2tv_1'(t)+(1+t^2)v_1''(t)| \leq C(1+t^2)^{-1}$. Now since $\Delta \geq |t_2| \geq C$, the integral in (25) is bounded. Thus

$$\left| \int_{t_0}^{b'} \frac{1}{1+t^2} e^{\mathbf{i}kz_2 v(t)} dt \right| \leq C(kh)^{-1}. \tag{25}$$

This completes the proof by combining the above estimate with (23)-(24). □

Lemma 4.9. *Let $a, b \in \mathbb{R}, a < b$. For any $x_r \in \Gamma_0^d, z \in \Omega$, we have,*

$$\left| \int_{\Gamma_0^{(a,b)}} \frac{\partial \Phi(x_s, z)}{\partial x_2(x_s)} u^s(x_r, x_s) e^{-2\mathbf{i}kx_{1s}} ds(x_s) \right| \leq C(1+\|\mathbb{S}\|)(kh)^{-1},$$
$$\left| \int_{\Gamma_0^{(a,b)}} \frac{\partial \Phi(x_r, z)}{\partial x_2(x_r)} u^s(x_r, x_s) e^{-2\mathbf{i}kx_{1r}} ds(x_r) \right| \leq C(1+\|\mathbb{S}\|)(kh)^{-1},$$

where C may be dependent on $kd_D, \|n(\cdot)\|_{L^\infty(D)}$, but is independent of k, h, d_D, a, b.

Proof. We only prove the first estimate. The second one is similar. Let

$$w(y,z) = \int_{\Gamma_0^{(a,b)}} \frac{\partial \Phi(x_s, z)}{\partial x_2(x_s)} u^s(y, x_s) e^{-2\mathbf{i}kx_{1s}} ds(x_s), \quad \forall y \in \mathbb{R}^2_+, \tag{26}$$

be the linear superposition of the scattering wave $u^s(\cdot, x_s)$ along the source direction. Then $w(y,z)$ is the scattering solution to (12) with

$$g(y,z) = \int_{\Gamma_0^{(a,b)}} \frac{\partial \Phi(x_s, z)}{\partial x_2(x_s)} N(y, x_s) e^{-2\mathbf{i}kx_{1s}} ds(x_s).$$

By Lemma 4.8, we have $|g(y,z)| \leq C(kh)^{-1}$. By the integral representation theorem

$$w(x_r, x_s) = k^2 \int_D [n(y)-1] N(x_r, y)[w(y, x_s) + g(y, x_s)] ds(y).$$

By Lemma 3.1, we have

$$\begin{aligned} |w(x_r,z)| \leq & k^2 \|n(\cdot)\|_{L^\infty(D)} \|N(x_r,\cdot)\|_{L^2(D)} (\|\mathbb{S}\| \|g\|_{L^2(D)} + \|g(x_s,\cdot)\|_{L^2(D)}) \\ \leq & C(1+\|\mathbb{S}\|)(kh)^{-1}. \end{aligned} \tag{27}$$

This completes the proof. □

Lemma 4.10. *We have*

$$\begin{aligned} & \left| \iint_{\Gamma_0^d \times \Gamma_0^d \setminus \bar{Q}_\delta} \frac{\partial \Phi(x_s, z)}{\partial x_2(x_s)} \frac{\partial \Phi(x_r, z)}{\partial x_2(x_r)} \frac{u^s(x_r, x_s) \overline{u^i(x_r, x_s)}}{u^i(x_r, x_s)} ds(x_r) d(x_s) \right| \\ \leq & C(1+\|\mathbb{S}\|)(kh)^{-1/2}. \end{aligned} \tag{28}$$

where C may be dependent on $kd_D, \|n(\cdot)\|_{L^\infty(D)}$, but is independent of k, h, d_D.

Proof. Notice that $u^i(x_r, x_s) = 2\Phi(x_r, x_s)$, by the asymptotic formula (21), we have

$$\frac{\overline{u^i(x_r, x_s)}}{u^i(x_r, x_s)} = -e^{-2\mathbf{i}k|x_r - x_s| + \mathbf{i}\frac{\pi}{2}} + \rho_0(x_r, x_s), \quad |\rho_0(x_r, x_s)| \leq C(k|x_r - x_s|)^{-1}.$$

Since $k|x_r - x_s| \geq C\sqrt{kh}$ for $x_r, x_s \in \Gamma_0^d \times \Gamma_o^d \backslash \bar{Q}_\delta$, by Lemma 4.3 and Lemma 4.4 we have

$$\begin{aligned}(29)\qquad &\left| \iint_{\Gamma_0^d \times \Gamma_0^d \backslash \bar{Q}_\delta} \frac{\partial \Phi(x_s, z)}{\partial x_2(x_s)} \frac{\partial \Phi(x_r, z)}{\partial x_2(x_r)} u^s(x_r, x_s) \rho_0(x_r, x_s) ds(x_r) d(x_s) \right| \\ &\leq C(1 + \|\mathbb{S}\|)(kh)^{-\frac{1}{2}}.\end{aligned}$$

We are now estimating the following integral

$$\begin{aligned}(30)\qquad &\iint_{\Gamma_0^d \times \Gamma_0^d \backslash \bar{Q}_\delta} \frac{\partial \Phi(x_r, z)}{\partial x_2(x_r)} \frac{\partial \Phi(x_s, z)}{\partial x_2(x_s)} u^s(x_r, x_s) e^{-2\mathbf{i}k|x_r - x_s|} ds(x_r) ds(x_s) \\ &= \int_{-d}^{d-\delta} \frac{\partial \Phi(x_r, z)}{\partial x_2(x_r)} \left[\int_{x_{1r}+\delta}^{d} \frac{\partial \Phi(x_s, z)}{\partial x_2(x_s)} u^s(x_r, x_s) e^{-2\mathbf{i}k(x_{1s} - x_{1r})} dx_{1s} \right] dx_{1r} \\ &\quad + \int_{-d}^{d-\delta} \frac{\partial \Phi(x_s, z)}{\partial x_2(x_s)} \left[\int_{x_{1s}+\delta}^{d} \frac{\partial \Phi(x_r, z)}{\partial x_2(x_r)} u^s(x_r, x_s) e^{-2\mathbf{i}k(x_{1r} - x_{1s})} dx_{1r} \right] dx_{1s} \\ &:= \mathrm{IV}_1 + \mathrm{IV}_2.\end{aligned}$$

By Lemma 4.9, we have

$$\left| \int_{x_{1r}+\delta}^{d} \frac{\partial \Phi(x_s, z)}{\partial x_2(x_s)} u^s(x_r, x_s) e^{-2\mathbf{i}k x_{1s}} dx_{1s} \right| \leq C(1 + \|\mathbb{S}\|)(kh)^{-1}.$$

By Lemma 4.4 we have $|\mathrm{IV}_1| \leq C(1+\|\mathbb{S}\|)(kh)^{-1/2}$. Similarly, we can prove $|\mathrm{IV}_2| \leq C(1 + \|\mathbb{S}\|)(kh)^{-1/2}$. This completes the proof by combining with (29)-(30). □

Now we are in the position to prove the main theorem of this section.

Proof of Theorem 4.1. The theorem now follows from (16), Lemma 4.5, Lemma 4.6 and Lemma 4.10. □

5. **Extensions.** In this section we consider the reconstruction of sound-soft and impedance obstacles in the half space with phaseless data. For sound-soft obstacles, the measured data $|u(x_r, x_s)| = |u^s(x_r, x_s) + N(x_r, x_s)|$, where $u^s(x_r, x_s)$ is the scattering solution of the following problem,

$$\begin{aligned}(31)\qquad &\Delta u^s + k^2 u^s = 0 && \text{in } \mathbb{R}^2_+ \backslash \bar{D},\\ (32)\qquad &u^s(x, x_s) = -N(x, x_s) && \text{on } \Gamma_D,\\ (33)\qquad &\frac{\partial u^s}{\partial x_2}(x, x_s) = 0 && \text{on } \Gamma_0.\end{aligned}$$

By modifying the argument in Section 4 we can show the following theorem whose proof is omitted.

Theorem 5.1. *If the measured field $|u(x_r, x_s)| = |u^s(x_r, x_s) + N(x_r, x_s)|$ with $u^s(x_r, x_s)$ satisfying (31) − (33), we have*

$$I_{\mathrm{RTM}}^{\mathrm{phaseless}}(z) = I_{\mathrm{RTM}}(z) + R_{\mathrm{RTM}}^{\mathrm{phaseless}}(z), \quad \forall z \in \Omega,$$

where

$$\left| R_{\mathrm{RTM}}^{\mathrm{phaseless}}(z) \right| \leq C(1 + \|\mathbb{S}\|)^2 (kh)^{-\frac{1}{2}}, \quad \forall z \in \Omega.$$

Here $\mathbb{S}$ is the Dirichlet to Neumann map, and the constant C may depend on $kd_D, \|n(\cdot)\|_{L^\infty(D)}$, but is independent of k, h, d_D.

For impedance obstacles, the measured data $|u(x_r,x_s)| = |u^s(x_r,x_s)+N(x_r,x_s)|$, where $u^s(x_r,x_s)$ is the scattering solution of the following problem,

$$\Delta u^s + k^2 u^s = 0 \quad \text{in} \quad \mathbb{R}^2_+ \backslash \bar{D}, \tag{34}$$

$$\frac{\partial u^s}{\partial \nu} + \mathbf{i}k\eta(x)u^s = -\left(\frac{\partial}{\partial \nu} + \mathbf{i}k\eta(x)\right) N(x,x_s) \quad \text{on} \quad \Gamma_D, \tag{35}$$

$$\frac{\partial u^s}{\partial x_2}(x,x_s) = 0 \quad \text{on} \quad \Gamma_0. \tag{36}$$

By modifying the argument in Section 4 we can show the following theorem whose proof is omitted.

Theorem 5.2. *If the measured field* $|u(x_r,x_s)| = |u^s(x_r,x_s) + N(x_r,x_s)|$ *with* $u^s(x_r,x_s)$ *satisfying* (34) – (36), *we have*

$$I_{\mathrm{RTM}}^{\mathrm{phaseless}}(z) = I_{\mathrm{RTM}}(z) + R_{\mathrm{RTM}}^{\mathrm{phaseless}}(z), \quad \forall z \in \Omega,$$

where

$$\left|R_{\mathrm{RTM}}^{\mathrm{phaseless}}(z)\right| \le C(1+\|\mathbb{S}\|)^2 (kh)^{-\frac{1}{2}}, \quad \forall z \in \Omega.$$

Here $\mathbb{S}$ *is the Dirichlet to Neumann map, and the constant* C *may depend on* $kd_D, \|n(\cdot)\|_{L^\infty(D)}$, *but is independent of* k, h, d_D.

For sound-soft or impedance obstacles, the studies in [10] show that the imaging function I_{RTM} will peak at the boundary of the scatterer if $kh \gg 1$ and $d \gg h$. Therefore we again expect the imaging function $I_{\mathrm{RTM}}^{\mathrm{phaseless}}(z)$ will have contrast on the boundary of the scatterer and decay outside the scatterer also for imaging impedance or sound-soft scatterers.

6. **Numerical examples.** In this section, we show several numerical examples by using the synthesized scattering data which are computed by standard Nyström methods. We use a uniform mesh with ten points per wavelength over the boundary to solve the boundary integral equation. The boundaries of the obstacles used in our numerical experiments are parameterized as follows:

$$\begin{aligned}
&Circle: \quad x_1 = \rho\cos\theta, \quad x_2 = \rho\sin\theta,\\
&p-leaf: \quad x_1 = r(\theta)\cos\theta, \quad x_2 = r(\theta)\sin\theta, \quad where \quad r(\theta) = 1 + 0.2\cos(p\theta),\\
&Peanut: \quad x_1 = \cos\theta + 0.2\cos 3\theta, \quad x_2 = \sin\theta + 0.2\sin 3\theta,\\
&Rounded \ \ square: \quad x_1 = \cos^3\theta + \cos\theta, \quad x_2 = \sin^3\theta + \sin\theta.
\end{aligned}$$

In all our examples, we always choose $h = 10$ and $d = 50$. The sources x_s and receivers x_r are uniformly distributed on Γ_0^d with

$$x_{1s} = -d + \frac{2d}{N_s}(s-1) + \frac{d}{N_s}, \quad x_{1r} = -d + \frac{2d}{N_r}(r-1),$$

where $s = 1,\dots,N_s, r = 1,\dots,N_r$.

Example 6.1. We consider the imaging of penetrable obstacles with different shapes including circle, peanut, kite and rounded square using phaseless data. Let the diffraction index $n(x) = 1$ outside D and $n(x) = 0.5$ inside D. The sampling domain is $\Omega = [-2,2] \times [8,12]$, with uniform mesh 201×201. The probe wave number is $k = 4\pi$, and $N_s = 512$, $N_r = 512$.

The top row of Figure 1 shows the imaging results of penetrable obstacles with different shapes. We observe that the location and upper boundary of the obstacle can be found effectively for different shapes. The interesting point is that the lower

boundary of obstacles can also be imaged due to the diffraction energy back to the receivers after penetrating the media. As a comparison, we also compute the imaging results with the full phase scattering data which is shown in the bottom row of Figure 1. The imaging results with our method using phaseless data are almost the same as results using full phase scattering data, which confirms our theory in this paper.

Example 6.2. We consider the imaging of an ellipse like obstacle with different boundary conditions, including sound soft, sound hard and impedance boundary with $\eta = 1$. The sampling domain is $\Omega = [-2, 2] \times [8, 12]$ with the uniform mesh 201×201. The probe wave number is $k = 4\pi$ and $N_s = 512$, $N_r = 512$.

Figure 2 shows that the location and upper boundary of the obstacles with different boundary conditions can be found without knowing any phase information of the data. Unlike the penetrable obstacle, the lower boundary of the obstacles can not be located as the scattering signals induced by the lower part of the obstacle propagate out without being recorded by receivers.

Example 6.3. We consider the stability of our imaging algorithm with respect to the additive Gaussian random noises in two tests using single frequency and multifrequency data. We introduce the additive Gaussian noise as follows,

$$|u|_{noise} = |u| + v_{noise},$$

where

$$v_{noise} = \mu \max |u| \epsilon, \quad and \quad \epsilon \sim N(0, 1).$$

The sampling domain is $\Omega = [-2, 2] \times [8, 12]$, with the uniform mesh 201×201. We assume $N_s = 256$, $N_r = 256$, and the wave number $k = 4\pi$, or $k = 2\pi \times [1 : 0.25 : 3]$.

In our first test, we choose a single penetrable obstacle as the imaging object and the probe wavenumber is $k = 4\pi$ for imaging with single frequency data. The top row of Figure 3 shows the imaging results with the noise level $\mu = 10\%, 20\%, 30\%, 40\%$ in the single frequency scattered phaseless data, respectively. The imaging results are still quite stable with the increasing of the noise level. We then generate multi-frequency data using the probe wavenumber $k = 2\pi \times [1 : 0.25 : 3]$. As shown in the bottom row of Figure 3, the noise has been sucessfully suppressed and some undesired oscillations in imaging result with single frequency data are also cancelled by using multi-frequency data, which improves the imaging resolution of the imaging result.

For the second test, we choose two sound soft obstacles as imaging objects and the probe wavenumer is $k = 4\pi$ for imaging with single frequency data. The search domain is $\Omega = [-5, 5] \times [6, 16]$ with a sampling mesh 201×201. The results shown in Figure 4 are imaged with phaseless data correlated with the nosie level as our previous test from left to right. Similarly, we also observe the noise can be suppressed and imaging results are improved by using multi-frequecy data.

Example 6.4. We switch the position of two obstacles in **Example 6.3** to show the impact of the limited data acquisition aperture. All the parameters are the same as in **Example 6.3**. The top row in Figure 5 are imaging results of two closely located obstacles with single frequency data (left plot) and multi-frequency data (right plot). We observe that the upper boundary of the larger obstacle is imaged as expected, but the smaller elliptic one below is completely invisible even we use the multi-frequency data. In the bottom row of Figure 5, we show the imaging results when these two obstacles are separated with a larger distance. We

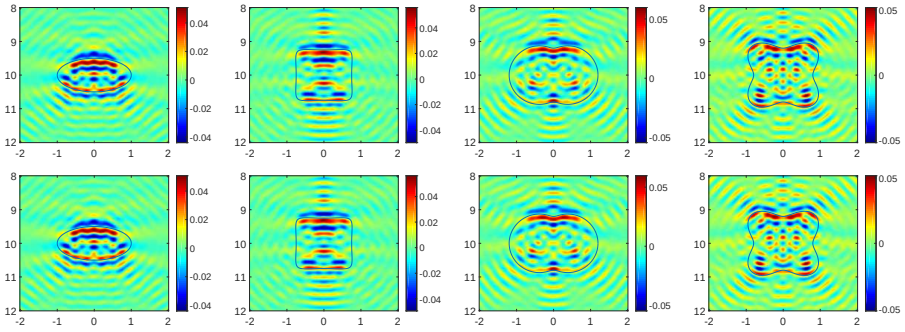

FIGURE 1. Examples 6.1: Imaging results of penetrable obstacles with different shapes from left to right. The top results are imaged with phaseless data by our RTM algorithm, and the bottom one are imaing results with full phase data. The probe wave number is $k = 4\pi$, and $N_s = 512$, $N_r = 512$.

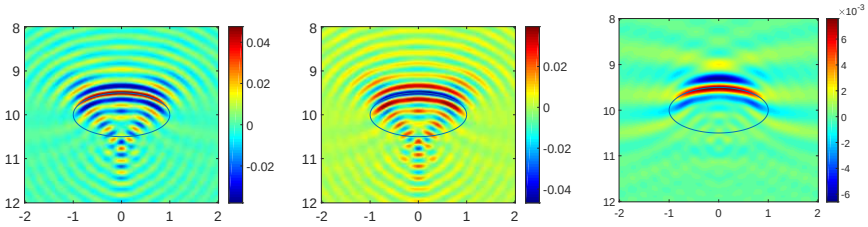

FIGURE 2. Example 6.2: Imaging results of an elliptic obstacle with boundary conditions as sound soft, sound hard and impedance boundary with $\lambda = 1$, respectively. The probe wave number $k = 4\pi$, and $N_s = 512$, $N_r = 512$.

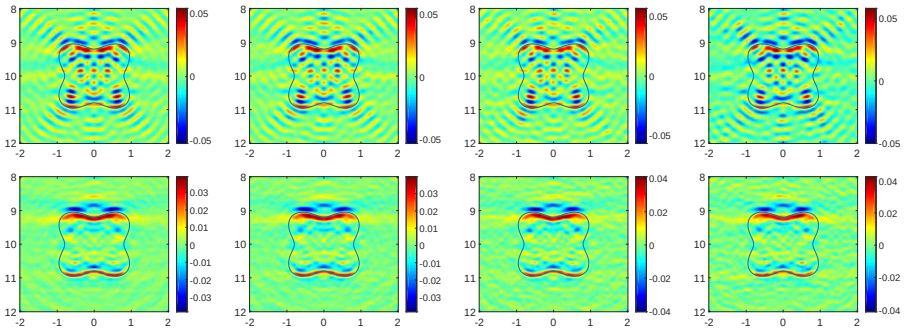

FIGURE 3. Examples 6.3 (first test): Imaging results of a penetrable obstacle with noise levels $\mu = 0.1, 0.2, 0.3, 0.4$ (from left to right). The top row is imaged with single frequency data, and the bottom row is imaged with multi-frequency data.

can image the upper boundary of the elliptic obstacle below even only using single frequency data. The imaging result is also improved by using multi-frequency data. This indicates that the bottom obstacle can be imaged as long as the incident waves

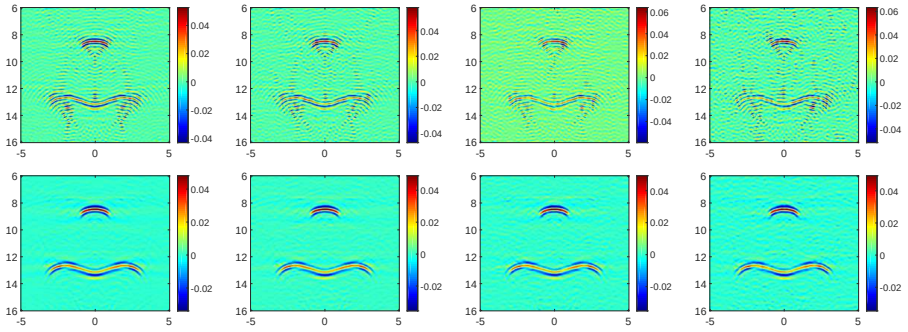

Figure 4. Example 6.3 (second test): Imaging results of two sound soft obstacles. All the parameters are the same as that in Figure 3.

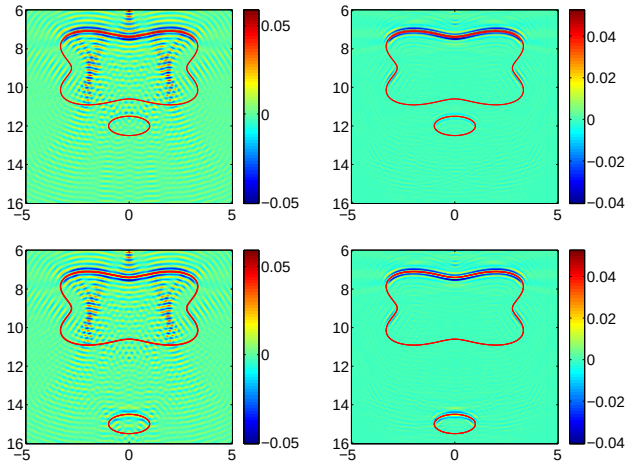

Figure 5. Example 6.4: Imaging results of two sound soft obstacles overlaid with the true obstacle model. The left column is imaged with the single frequency data, and the right one is imaged with the multi-frequency data.

are not blocked by the larger top obstacle and the reflected wa ves can be acquisited on the surface.

REFERENCES

[1] G. Bao, P. Li and J. Lv, Numerical solution of an inverse diffraction grating problem from phaseless data, *J. Opt. Soc. Am. A*, **30** (2013), 293–299.

[2] P. Bardsley and F. Vasquez, Kirchhoff migration without phases, *Inverse Problems,* **32** (2016), 105006, 17 pp.

[3] N. Bleistein, J. Cohen and J. Stockwell, *Mathematics of Multidimensional Seismic Imaging, Migration, and Inversion*, Springer, New York, 2001.

[4] F. Cakoni and D. Colton, *A Qualitative Approach to Inverse Scattering Theory*, Applied Mathematical Sciences 188, Springer, New York, 2014.

[5] A. Chai, M. Moscoso and G. Papanicolaou, Array imaging using intensity-only measurements, *Inverse Problems*, **27** (2010), 015005, 16pp.

[6] S. N. Chandler-Wilde, I. G. Graham, S. Langdon and M. Lindner, Condition number estimates for combined potential boundary integral operators in acoustic scattering, *J. Integral Equa. Appli.*, **21** (2009), 229–279.
[7] J. Chen, Z. Chen and G. Huang, Reverse time migration for extended obstacles: Acoustic waves, *Inverse Problems*, **29** (2013), 085005, 17pp.
[8] J. Chen, Z. Chen and G. Huang, Reverse time migration for extended obstacles: Electromagnetic waves, *Inverse Problems*, **29** (2013), 085006, 17pp.
[9] Z. Chen and G. Huang, Reverse time migration for extended obstacles: Elastic waves (in Chinese), *Sci. Sin. Math.*, **58** (2015), 1811–1834.
[10] Z. Chen and G. Huang, Reverse time migration for reconstructing extended obstacles in the half space, *Inverse Problems*, **31** (2015), 055007, 19pp.
[11] Z. Chen and G. Huang, Phaseless imaging by reverse time migration: Acoustic waves, *Numer. Math. Theor. Meth. Appl.*, **10** (2017), 1–21.
[12] Z. Chen and G. Huang, A direct imaging method for electromagnetic scattering data without phase information, *SIAM J. Imag. Sci.*, **9** (2016), 1273–1297.
[13] A. J. Devaney, Structure determination from intensity measurements in scattering experiments, *Physical Review Letters*, **62** (1989), 2385–2388.
[14] M. Ďurso, K. Belkebir, L. Crocco, T. Isernia and A. Litman, Phaseless imaging with experimental data: Facts and challenges, *J. Opt. Soc. Am. A,* **25** (2008), 271–281.
[15] G. Franceschini, M.Donelli, R. Azaro and A. Massa, Inversion of phaseless total field data using a two-step strategy based on the iterative multiscaling approach, *IEEE Trans. Geosci. Remote Sens.*, **44** (2006), 3527–3539.
[16] L. Grafakos, *Classical and Modern Fourier Analysis*, Pearson, London, 2004.
[17] O. Ivanyshyn and R. Kress, Identification of sound-soft 3D obstacles from phaseless data, *Inverse Problem and Imaging*, **4** (2010), 131–149.
[18] O. Ivanyshyn and R. Kress, Inverse scattering for surface impedance from phase-less far field data, *Journal of Computational Physics*, **230** (2011), 3443–3452.
[19] R. Kress and W. Rundell, Inverse obstacle scattering with modulus of the far field pattern as data, H. W. Engl et al. (eds.), *Inverse Problems in Medical Imaging and Nondestructive Testing*, Springer, Vienna, (1997), 75–92.
[20] J. Li and J. Zou, A direct sampling method for inverse scattering using far-field data, *Inverse Problems and Imaging*, **7** (2013), 757–775.
[21] J, Li, H. Liu, Z. Shang and H. Sun, Two single-shot methods for locating multiple electromagnetic scatterers, *SIAM J. Appl. Math.*, **73** (2013), 1721–1746.
[22] J, Li, H. Liu and Q. Wang, Locating multiple multiscale electromagnetic scatterers by a single far-field measurement, *SIAM J. Imag. Sci.*, **6** (2013), 2285–2309.
[23] J, Li, H. Liu and J. Zou, Locating multiple multiscale acoustic scatterers, *Multiscale Modeling and Simulation*, **12** (2014), 927–952.
[24] A. Novikov, M. Moscoso and G. Papanicolaou, Illumination strategies for intensity-only imaging, *SIAM J. Imag. Sci.*, **8** (2015), 1547–1573.
[25] G. N. Watson, *A Treatise on the Theory of Bessel Functions*, Cambridge University Press, Cambridge, 1995.
[26] Y. Zhang and J. Sun, Practicle issues in reverse time migration: True amplitude gathers, noise removal and harmonic source encoding, *First Break,* **26** (2009), 29–35.
[27] Y. Zhang, S. Xu, N. Bleistein and G. Zhang, True-amplitude, angle-domain, common-image gathers from one-way wave-equation migration, *Geophysics*, **72** (2007), S49–S58.

Received for publication December 2016.

E-mail address: zmchen@lsec.cc.ac.cn
E-mail address: fangsf@lsec.cc.ac.cn
E-mail address: ghhuang@rice.edu